scientific reports

Check for updates

OPEN

Bioactive silver nanoparticles derived from *Carica papaya* floral extract and its dual-functioning biomedical application

E. S. Harsha Haridas, M. K. Ravi Varma & Goutam Kumar Chandra✉

Replacing synthetic phytochemicals with natural plant extracts for metal nanoparticle synthesis enable cost-effective, large-scale production with reduced environmental and health risks while enhancing biomedical efficacy. This study presents the green synthesis of silver nanoparticles (AgNPs) using a flavonol-enriched extract from male papaya flowers (KQE), an underutilized agricultural waste. Using 20% (v/v) KQE, highly stable, spherical KQ-AgNPs (12.3 ± 3.0 nm) were synthesized via in-situ generation of free radicals, such as ortho-quinones, which reduced Ag^+ ions. KQ-AgNPs exhibit superior antibacterial activity against both gram-positive and gram-negative bacteria compared to chemically synthesized AgNPs (AgNPs-Chem) and KQE alone. In vitro anticancer assays reveal enhanced cytotoxicity against breast carcinoma cells (MCF-7) with an IC_{50} of 21.25 ± 1.14 µg/mL, significantly lower than AgNPs-Chem (33.05 ± 3.13 µg/mL), while maintaining high biocompatibility with normal cells (HEK-293) with a greater IC_{50} of 169.96 ± 2.3 µg/mL. This study highlights the dual therapeutic potential of KQ-AgNPs, emphasizing their enhanced antibacterial and anticancer efficacy while exemplifying an innovative waste-to-wealth approach.

Keywords Ag nanoparticles, Antibacterial activity, Anticancer activity, Green synthesis, Papaya male flower

Silver nanoparticles (AgNPs) have gained significant attention in the biomedical field for their exceptional optical, electrical, antimicrobial, and anticancer properties. Numerous studies confirming the superior antimicrobial efficacy of AgNPs compared to Ag^+ ions alongside low toxicity[1–3]. Due to these unique features, the primary applications of AgNPs demand leveraging their antimicrobial and biomedical efficacy in developing medical devices, antibacterial agents, sensors, food preservation techniques, protective clothing and active packaging[4–7]. Researchers are giving special attention to synthesis methods for AgNPs that ensure minimal toxicity and maximum biocompatibility, prompting numerous studies to explore the fabrication using synthetic phytochemicals as alternatives to conventional reducing agents like sodium borohydride ($NaHB_4$) or sodium citrate ($Na_3C_6H_5O_7$)[8,9]. It is evident that while incorporating phytochemicals such as flavonoids, polyphenols, aminoacids or vitamins into MNPs, the bioavailability and inherent therapeutic properties of these metabolites are enhanced thereby increasing the biomedical activity of corresponding MNPs[10].

Kaempferol and quercetin are natural flavonols, with similar chemical features primarily found in vegetables, fruits and flowers. They are known for their diverse therapeutic efficacies, including antimicrobial, antioxidant, anti-inflammatory, and anticancer effects[11]. Almatroudi et al. have extensively demonstrated the anticancer potential of kaempferol, highlighting its ability to modulate various cell signalling pathways. Their findings reveal that kaempferol induces apoptosis and cell cycle arrest in cancer cells while activating tumour suppressor genes[12]. In a study D.H. Kim et al. demonstrated that quercetin regulates epigenetic mechanisms, influencing the expression of miRNAs and modulating DNA methylation to exert anticancer effects[13]. Independently, M. Kedhari Sundaram highlighted quercetin's ability to enhance the sensitivity of tumour cells to chemotherapy, further emphasizing its therapeutic value in cancer treatment[14]. However, direct interaction of synthetic kaempferol or quercetin with live cells has poor bioavailability, stability, and non-specific effects, limiting their therapeutic efficacy. Nanoformulations address these issues by enhancing solubility, stability, and targeted delivery while minimizing toxicity[10,15].

Research on the synthesis of AgNPs incorporating either kaempferol or quercetin has been extensively explored[15–18]; however, studies examining the simultaneous incorporation of both compounds remain limited.

Department of Physics, National Institute of Technology, Kozhikode, Kerala 673601, India. ✉email: goutam@nitc.ac.in

Anuar et al. critically assessed the antibacterial efficacy of kaempferol-infused AgNPs against methicillin-resistant *Staphylococcus* (MRSA) bacteria, demonstrating that the enhanced antibacterial activity of kaempferol-AgNPs compared to the bare AgNPs is due to the synergistic interaction between kaempferol and AgNPs[17]. However, the synthesized kaempferol- AgNPs were heterogeneous in both phases and structures. Additionally, numerous studies have also investigated the stabilizing effects of these chemical entities when combined with AgNPs. For instance, Deng et al. synthesized colloidal AgNPs in an ethanolic solution, achieving stability up to two months[10]. The smaller-sized NPs, approximately 10 nm in diameter, exhibited superior antibacterial activity against both gram-positive and gram-negative bacteria when compared to AgNPs synthesized using $NaBH_4$. Since the solvent medium is ethanol, the synthesizing approach is not favourable for large-scale production while considering biocompatibility as well as cost-effectiveness[18]. In a recent study, Bharathi et al., demonstrated a synthesis procedure for nanocomposite consisting of kaempferol, chitosan and Ag that exhibited a dose-depended antibacterial action against S. aureus and P. aeruginosa and potential inhibitory effects against triple-negative breast cancer with an IC_{50} of 53 µg/ml[19]. But those nanocomposites were unsuitable for practical application due to prolong acid treatment. In another study, Alyami et.al, investigated the cytotoxic effects of kaempferol-coated AgNPs (~ 200 nm) on HepG2 cells, observing a dose-dependent response in both cell viability and lactate dehydrogenase (LDH) leakage[20]. Despite the existing biomedical activities demonstrated by Ag-kaempferol composites, challenges such as complex medium or prolonged acid exposure, crystalline ambiguity, potential biomolecule degradation, reduced stability, and unintended toxicity underscore the necessity for alternative synthesis approaches[21].

Utilizing plant extracts rich in kaempferol or quercetin offer a more biocompatible and sustainable route for AgNP synthesis, enhancing stability and therapeutic efficacy while minimizing the drawbacks mentioned earlier[15,19–22]. Based on the study conducted by Mean et al., for determining total flavonoids and individual kaempferol and quercetin present in more than 20 selected plant varieties, *Carica papaya* (Papaya) stands out as an excellent candidate having high flavonoid content, particularly kaempferol (453.0 mg/kg) and quercetin (811.0 mg/kg)[23]. The obtained result was further supported by similar studies which determined the quantity of flavonoids in papaya leaves by Nugroho et al. Their study suggested that young leaves of papaya contain a high level of total flavonoids especially with quercetin, kaempferol and their derivatives as the main compounds[24].

India is one of the largest papaya producers in the world. As per studies, forecasts for the period from 2021 to 2030 indicate that the area under cultivation and papaya production in India are projected to reach 1,538 hectares and 6,384,220 metric tons, respectively, by 2030[25]. This anticipated growth highlights the ample availability of papaya and its byproducts. While compared to other plants, Papaya offers a balanced and substantial concentration of kaempferol and quercetin, enabling them as potent bioactive reducing and stabilizing agents, which are essential for efficient NP synthesis[26–33]. Although numerous studies have explored the use of various parts of the papaya tree for synthesizing MNPs, such as AgNPs, for biomedical applications, its abundance and sustainable availability make it an environmentally friendly and cost-effective option for green nanotechnology[33–35]. On the other end, male papaya trees, often overlooked due to their infertility, remain largely unutilized despite their superior richness in phytochemicals compared to female trees[26]. However, experimental evidence indicates that male papaya floral extracts exhibit greater phytochemical activity, attributed to higher concentrations of compounds such as kaempferol, quercetin, myricetin, and their glycosides[26–33].

In line with promoting a waste-to-wealth strategy in synthesis and ensuring cost-effectiveness and biocompatibility in product formation, we have used male papaya flowers to prepare the extract for synthesizing and stabilizing AgNPs (KQ-AgNPs). As prepared KQ-AgNPs were investigated for their potential towards antibacterial activity against both gram-positive as well as gram-negative clinical isolates and compared with that of pure KQE as well as chemically synthesized AgNPs (AgNPs-Chem). We have also evaluated the cell viability effects of KQ-AgNPs on both breast cancer cells (MCF-7) and Human Embryonic Kidney cells (HEK293).

Experimental

Plant materials

Fresh papaya male flowers were collected from the Vaibhav agro-farm of National Institute of Technology Calicut, Kerala, India. To ensure consistent flavonoid content and reproducibility in KQ-AgNPs synthesis and biological activity, male papaya flowers were collected from the same plant throughout the study. The collection of the plant material and the research work associated with this complies with relevant institutional, national, and international guidelines and legislation.

Chemicals

Silver nitrate ($AgNO_3$) and Sodium borohydride ($NaBH_4$) were purchased from Sigma-Aldrich Chemical Co (United States). Sodium hydroxide (NaOH) and Hydrochloric acid (HCl) were purchased from Nice Chemicals (Kerala, India). All chemicals were used without any further purification. All experiments were carried out using deionized (DI) water.

Preparation of KQE

Freshly plucked male papaya flowers were washed several times with DI water to remove the dust. 10 gm of washed flowers were squeezed using mortar and pestle and boiled with 250 ml of DI water at 100 °C for 5 min. As per literature evidences, quercetin exhibit its eight times greater than normal antioxidant activity in water soluble phases. Moreover, the aqueous solubility of quercetin enhances in boiling water (100 °C). Therefore these studies ensures our efficiency of extract preparation medium as well as temperature[36,37]. The extract was allowed to cool at room temperature. The obtained yellow color extract was filtered using Whatman No.1 filter paper of pore size 11 µm followed by filtration using syringe filter of pore size 0.22 µm and the supernatant

was stored at 4 °C for further studies. Prior to the synthesis of KQ-NPs, we have monitored the absorption characteristics of KQE to verify that the flavonoid content was constant across batches.

Preparation of KQ-AgNPs

Figure 1 represents schematic of procedure for the synthesis of KQ-AgNPs. The pH of KQE was measured to be 6.5. The formation of KQ-AgNPs was optimized under three different pH conditions: acidic (3), neutral (7), and basic (9), by adding appropriate amounts of NaOH, diluted HCl (1%). Furthermore, we have examined the formation of KQ-AgNPs with different composition ratios of Ag ions to KQE at basic pH. For a fixed Ag solution (10 mL, 10 mM), NPs formation was evaluated at 1, 2, 5, 10, 15, and 20% (v/v) KQE. The reaction mixtures were gently shaken and covered with aluminum foil to prevent photodegradation. Preliminary confirmation of KQ-AgNPs formation was indicated by a color change in the solution during the reaction, which was further monitored using UV–Vis absorption spectroscopy. The reaction mixtures were left overnight and centrifuged at 15,000 rpm for 10 min, with the process repeated three times using deionized (DI) water to remove impurities. The resulting black precipitate was dried at 60 °C in a vacuum oven for 3 h and then ground into a fine powder using a mortar and pestle after cooling to room temperature. The yield of KQ-AgNPs was highest at 20% (v/v) KQE, with a value of 78.76 ± 0.35%. The powdered KQ-AgNPs were stored in airtight sample bottles for further use. An appropriate amount of the powder was re-dispersed in DI water for subsequent studies.

Preparation of AgNPs-Chem

In our study for comparative analysis the chemically reduced AgNPs were synthesized by following the existing procedure reported by Khatoon et al.[7]. Briefly, a 0.6 M aqueous solution of $NaBH_4$ (20 mL) was heated at 70 °C for 20 min under continuous stirring. Subsequently, 80 mL of 10 mM $AgNO_3$ aqueous solution was added dropwise to the $NaBH_4$ solution. The temperature was then adjusted to 60 °C, and the mixture was stirred for 30 min. To prevent photo-degradation, the reaction vessel was covered with aluminum foil. After the reaction, the mixture was allowed to cool to room temperature and then centrifuged at 10,000 rpm for 10 min. The supernatant was carefully removed, and the resulting pellets were washed multiple times with deionized water to remove any residual reactants. The centrifugation and washing steps were repeated three times to ensure purity. The cleaned pellets were then dried at 30 °C, and the dried samples were ground into a fine powder. The powdered AgNPs were sealed in plastic containers for further characterization and analysis.

Characterization

As prepared samples were characterized with the aid of several experimental devices such as UV–visible and FTIR spectroscope. UV–visible absorption spectroscopy analysis results were performed on a double beam spectrophotometer (Model: UV-1800 Shimadzu, Make: Japan) of 1 nm resolution in the wavelength range 200–800 nm. The morphology and crystalline nature of as prepared KQ-AgNPs were examined by using a TEM (Model: FEI Tecnai G2 Spirit Bio-Twin, Make: USA) at an accelerating voltage of 300 kV and an ultra-high-resolution pole piece. Freshly prepared sample of appropriate dilution was drop casted on copper grid after ultra-sonication for TEM analysis. Morphological features of fixed bacteria samples (detailed procedure discussed in Supplementary Information) and elemental composition of KQ-AgNPs were analysed using FESEM/EDS facility (Model: Carl Zeiss Sigma 300, Make: Germany). Surface characterization of KQE and KQ–AgNPs was done using a FTIR spectrometer (Mode: PerkinElmer frontier, Make: USA) of attenuated total refection (FTIR–ATR) mode. Average hydrodynamic diameter of KQ-AgNPs was analyzed by using a particle size analyzer (Model: Malvern Nano ZS (4 mW, 633 nm), Make:UK). Zeta Check-Particle Charge Reader (Model: Microtrac, PMX 500, Make: Germany) was equipped for stability analysis of as prepared colloidal samples. Structural investigation of the KQ-AgNPs were done using XRD analyser (Model: Panalytical X'pert Pro MRD, Make: UK) with Cu Kα radiation (λ = 0.15418 nm) over a scanning range of 2θ (30°– 80°) and a step size of 0.02°.

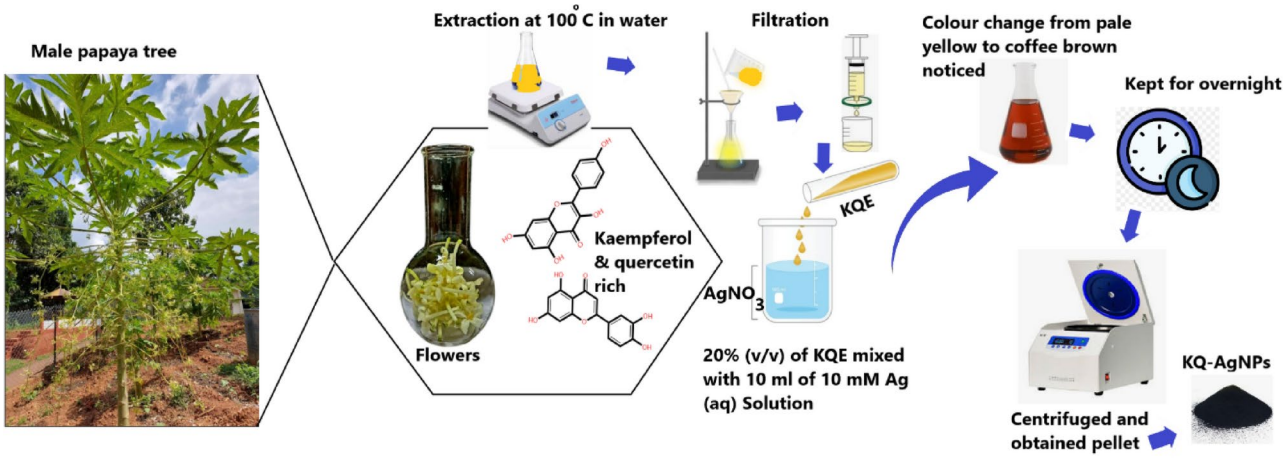

Fig. 1. Schematic representation KQ-AgNPs synthesis.

Results and discussion

Plant polyphenols, especially the phytochemicals found in different parts of the papaya plant, have attracted considerable interest for their capacity to chelate metal ions and their diverse applications, including antibacterial and anticancer properties[32,33]. These extracts function as competitive reducing and stabilizing agents. The bonding of phenolic compounds present in KQE with Ag^+ ions was monitored by noting the changes in the absorption spectra of KQE before and after the addition of Ag^+ ions. Figure 2a shows the UV–Vis absorption spectrum of KQE (Kaempferol-Quercetin Enriched extract) in an aqueous solution before its reaction with Ag^+ ions.

The spectrum exhibits two notable absorption features: a sharp peak at 272 nm and a shoulder around 330 nm. The sharp peak at 272 nm corresponds to Band II, which is associated with the benzoyl system. This band arises due to the $n \rightarrow \pi^*$ electronic transition localized between the A and C rings of kaempferol and quercetin molecules. The shoulder at around 330 nm corresponds to Band I, attributed to the cinnamoyl system. Band I is located in the range of 300–415 nm and serves as evidence of the $\pi \rightarrow \pi^*$ electronic transition within the B-ring, which is conjugated with the carbonyl group present in the C-ring[38].

Further we have investigated the reaction between KQE with aqueous $AgNO_3$ solution at three different pH conditions such as acidic, alkaline and neutral and corresponding absorption characteristics were noticed (Fig. 2b). In acidic conditions, the mixture showed agglomeration. In contrast, under basic conditions, the pale yellow solution turned dark coffee brown within 3 min, indicating rapid NP formation. For the neutral medium, the reaction proceeded very slowly, which normally give rise to larger sized NPs. Speisky et al. experimentally confirmed that at alkaline pH, both the oxidation rate and antioxidant activity of kaempferol, quercetin, and their derivatives are significantly higher[37]. From the Fig. 2b, it can be evident that compared to neutral pH at which reaction is quiet slow, the basic medium (pH = 9) is favourable for rapid formation of KQ-AgNPs with small size. Since KQE is abundant with flavonoids a large number of hydroxyl (-OH) groups which can deprotonate under alkaline conditions and enhances the formation of negatively charged ions. These increased electron density of free electrons further lowers the energy barrier for its oxidation by reducing the Gibbs free energy (ΔG). This reduction in ΔG facilitates the faster and efficient conversion of Ag^+ ions into AgNPs (e.g.,$Ag^+ + e^- \rightarrow Ag^0$) of reduced size so that aggregation is prevented. The experimental evidence presented by Chen et al. substantiates the hypothesis regarding the accelerated redox mechanisms of kaempferol in the presence of aminoacid residues[39]. However around physiological pH, the electrochemical intermediates produced by kaempferol and quercetin were unstable and proceed to form a stable final product in a quick manner. Since for metal ion reduction the availability reactive quinones are highly dependent, formation of KQ-AgNPs are slow at neutral pH[37,40,41].

To optimize the quantity of KQE required for the synthesis of KQ-AgNPs or to know the involvement of bioactive components present in KQE for the formation of KQ-AgNPs a series of reactions were carried out using a constant volume of aqueous $AgNO_3$ (10 ml) and varying the volume percentage of KQE (1%, 2%, 5%, 10%, 15%, and 20%). It was observed that higher concentrations of KQE accelerated the reaction rate and resulted in more symmetric SPR peaks, as illustrated in Fig. 2c. Notably, when 20% KQE was added to the aqueous solution of $AgNO_3$, the reaction mixture turned brown within 8 min, providing visible confirmation of KQ-

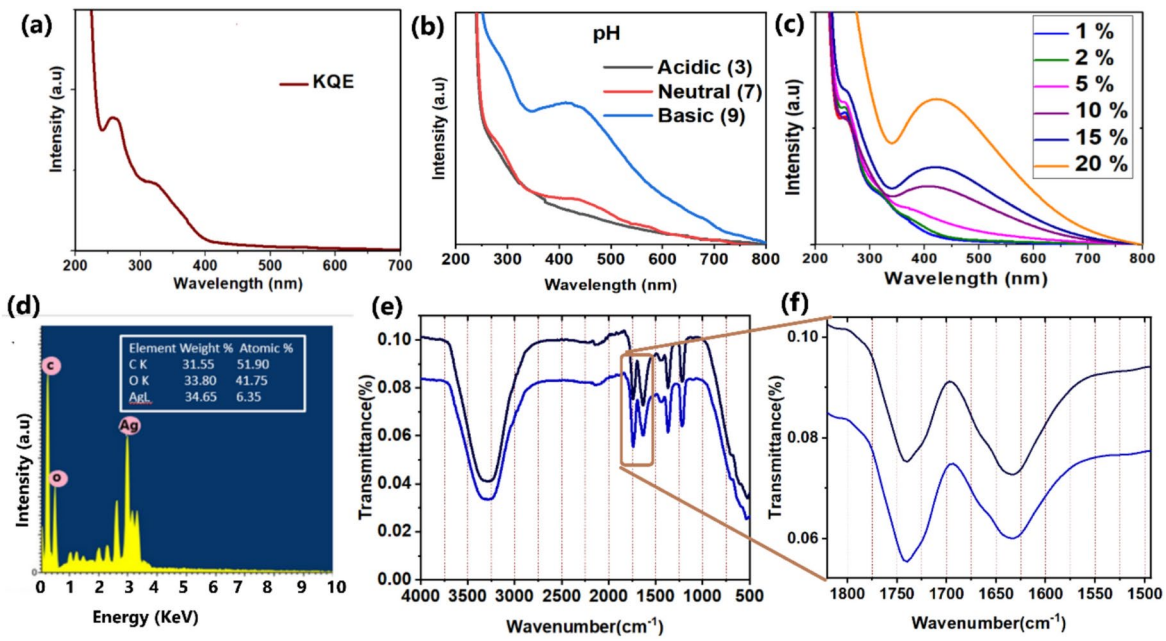

Fig. 2. UV–Vis spectrum of (**a**) KQE, KQ-AgNPs formed at various (**b**) pH and (**c**) KQE volume compositions (1, 2, 5, 10 & 20% (v/v)). (**d**) EDX spectrum of KQ-AgNPs and (**e**) FT-IR spectra of KQE (black line), KQ-AgNPs (red line) and ((i-ii) enlarged region from1800 to1500 cm^{-1}).

AgNPs formation. Elemental analysis of the corresponding sample (Fig. 2d) revealed a composition of biogenic elements (C and O) alongside the Ag metal core, with 31.55%, 33.80%, and 34.65%, respectively. Interestingly, our results contrast with previous studies conducted by Alyami et al., where kaempferol, when chemically incorporated into AgNPs, resulted in carbon dominance over silver. This disparity may be attributed to the higher concentration of kaempferol, which could reduce the silver content in those AgNPs and increase the carbon composition due to the structural features of kaempferol[17]. On the other hand, in another study where quercetin-functionalized AgNPs were synthesized by Maghsoodloo et.al, the carbon content was significantly low, below 10%, indicating that the synthesized AgNPs had less bioactive coverage[15]. Therefore, our KQ-AgNPs exhibit a balanced elemental composition, ensuring adequate bioactive coverage and stability. From Fig. 2c, it is evident that as the concentration of KQE increases from 5 to 20%, the SPR peak intensity of KQ-AgNPs rises significantly, indicating enhanced NP synthesis. This improvement is attributed to the higher availability of bioactive compounds in KQE, which act as efficient reducing and capping agents. However, at higher KQE concentrations, a broadening and slight shift in the SPR band were observed, suggesting potential NP agglomeration and polydispersity[42,43]. Consequently, further increases in KQE concentration were avoided to maintain NP stability. The KQ-AgNPs produced at 20% KQE displayed a well-balanced elemental composition (Fig. 2d) and attained an impressive yield of 78.76 ± 0.35%, notably surpassing previously documented yields. In optimized conditions, a yield of 53.31% was achieved with 29.22% of *Rubus discolor* leaf extract for the synthesis of AgNPs, necessitating elevated temperatures and extended reaction durations[44]. The effectiveness and sustainability of the current approach are highlighted by this comparison, which also highlights its potential as a time- and energy-efficient green synthesis technique.

Figure 2e represents the FTIR spectra of KQE (black line) and KQ-AgNPs (blue line) which deliver vital information about the surface chemistry of our KQ-AgNPs. Since KQE is enriched with flavonoids, it is very probable that the interactions of those moieties with surroundings will be effectively reflects as spectral changes related to hydroxyl and carbonyl vibrations[15]. The complex character of biological materials present in the control KQE reflects in the vibrational spectrum with dominated bands at 3300, 1740, 1635, 1445, 1370 and 1215 cm^{-1}. The first broad and dominant band at around 3300 cm^{-1} corresponds to stretching vibrations of hydroxyl moieties. The second band is due to C=O stretching vibrations of esters[1,17]. Similar band at 1740 cm^{-1} can also see from onion peel extract that contains superior quantity of quercetin and kampferol groups in it[45]. The third band can be associated with the C–C stretching vibrations of A-ring of both kampferol and quercetin[5,46,47]. The presence of aromatic benzene ring vibrations of kampferol and quercetin like flavonoids evident from the band at 1445 cm^{-1}.The asymmetric deformations of CH_3 groups can also associated with this band. C–OH bending in the B-ring of flavonoid moieties can be visible at 1370 cm^{-1}[46,47]. The band at 1215 cm^{-1} can be attributed to the stretching vibrations of C-rings[47]. Figure 2f shows that KQ-AgNPs exhibit a remarkable difference in the vibrational bands at 1740 and 1635 cm^{-1} to that of KQE. After the formation of KQ-AgNPs, the intensity of 1740 cm^{-1} get increased but a decrement is evident for the band at 1635 cm^{-1} (as depicted in the Fig. 2e (i & ii). Notably, the C=O/OH groups and catechol moieties in kaempferol-like flavonoids are known to be the most sensitive sites for metal interactions, as validated by Simunkova et al. in their study on Kaempferol-Cu^{2+} interactions[48]. These vibrational characteristics of KQ-AgNPs indicate the active role of dominant flavonoids in KQE during NPs synthesis. Additionally, the observed spectral changes before and after NP formation align with previous reports on AgNPs synthesized via green methods using extracts of tomato, onion, acacia catechu, and combined extracts as reducing and stabilizing agents, confirming effective flavonol interactions in the coordination redox reaction with metal ions[49].

Moreover, our method demonstrates uniform NP morphology, as evidenced by the TEM results (Fig. 3a, b), with a narrow size distribution and an average diameter of 12.3 ± 3.0 nm (Fig. 3c). Assuming all nanoparticles formed are uniform spheres, the approximate number of KQ-AgNPs produced in 1 ml of our sample is 4.88×10^{12} (calculation is given in Supplementary Information). The HR-TEM highlights the crystalline nature of the KQ-AgNPs, with lattice fringes corresponding to the (111) plane of Ag (Fig. 3b)[5,10]. The surface charge of the KQ-AgNPs was measured at different concentrations of KQE (10%, 15%, and 20%) and over various time durations (1 day, 1.5 months, and 3 months). A higher surface charge was observed at 20% KQE, indicating greater stability, with the zeta potential remaining consistent over three months (Fig. 3d)[10]. These findings align with the surface charge characteristics of $NaBH_4$ reduced AgNPs synthesized by Khatoon et al. for antimicrobial and cytotoxicity studies[7]. The size distribution obtained by DLS shows an average hydrodynamic diameter of 66.5 ± 1.6 nm, with a polydispersity index (PDI) of 0.445 (Fig. 3e) (DLS analysis of KQ-AgNPs prepared by using 10 and 15% of KQE is given in Figure S1 of SI). This larger size compared to the TEM analysis is attributed to the hydrodynamic shell formed by the capping agents (KQE) around the NPs[43]. Our results are align with previous studies conducted by Deng et al.[10].This highlights the potential of KQE in green nanotechnology for producing stable KQ-AgNPs with minimal environmental impact. Our methodology therefore, presents a significant advantage, as AgNPs are traditionally unstable and particularly prone to oxidation. However, to maintain consistent biochemical interactions and prevent aggregation or morphological changes during scale-up, careful process standardization and optimization are required.

The XRD pattern (Fig. 3f) exhibits prominent diffraction peaks at 2θ values of 38.1°, 44.3°, 64.5°, and 77.5°, corresponding to the (111), (200), (220), and (311) planes, respectively further validate the formation of highly crystalline AgNPs with prominent peaks indicative of the FCC structure[5,43]. These findings collectively establish that the use of 20% KQE optimizes the synthesis process and highest yields KQ-AgNPs with improved structural and stability characteristics, making it a promising method for future applications.

Mechanism of formation of KQ-AgNPs

The synthesis of MNPs induced by free radicals is well-documented[5,43,50]. In this study, we propose that the in-situ generation of free radicals, such as ortho-quinones formed during the oxidation of polyphenols in KQE,

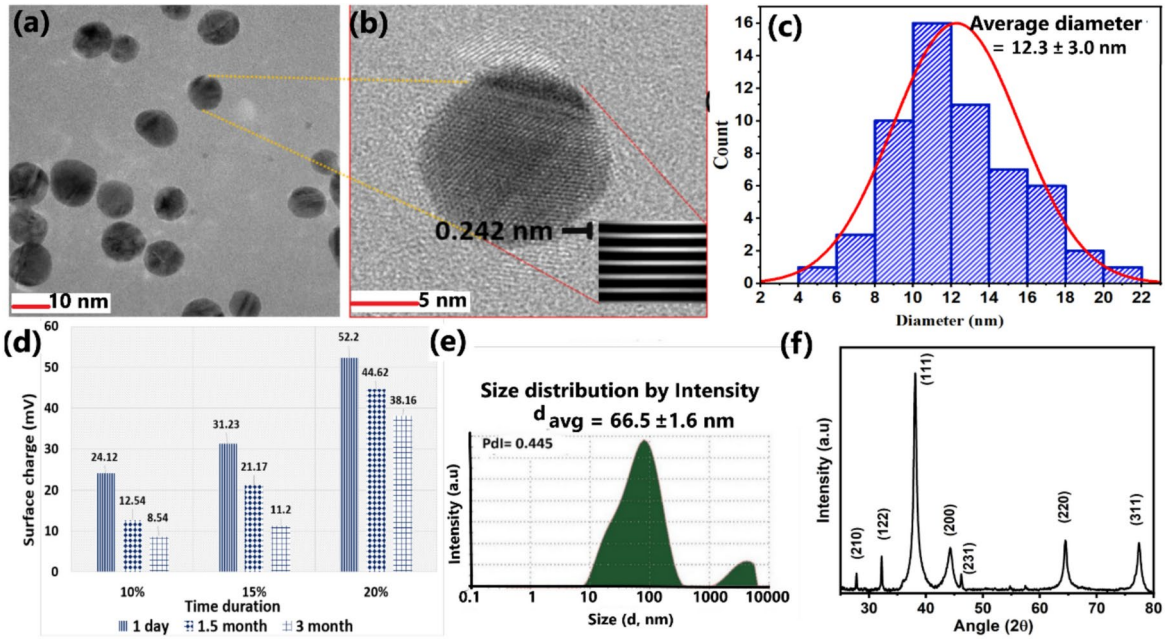

Fig. 3. (**a**) TEM and (**b**) HR-TEM (inset: lattice fringes) images of KQ-AgNPs. (**c**) size distribution histogram (**d**) surface charge analysis for time durations 1 day, 1.5 month & 3 month. (**e**) DLS spectrum and (**f**) XRD pattern for KQ-AgNPs.

facilitates the reduction of Ag salts to form KQ-AgNPs. Figure 4 illustrates the schematic representation for the plausible mechanism of formation as well as stabilization of KQ-AgNPs by the surface functional groups present in KQE. According to Van et al., KQE contains bioactive flavonoids, including kaempferol, quercetin, myricetin, and their glycosides (e.g., Kaempferol 3-O-α-L-rhamnopyranoside and Quercetin 3-O-β-D-galactopyranoside)[27]. These flavonoids are structured with three cyclic carbon rings: two benzene rings (A and B) linked by a heterocyclic pyran ring (C). Kaempferol and quercetin, are polyhydroxyflavonols, differ in their B-ring substituents: kaempferol has a phenol group, while quercetin contains a catechol group, which provides stronger antioxidant properties[11]. The electrochemical oxidation potential of kaempferol, quercetin and Ag are in the range of ~ 0.3–0.5, ~ 0.2–0.4 and ~ 0.7996 V respectively[11,37,43]. Since quercetin contains one additional hydroxyl group than kaempferol, it may be acting as stronger reducing agent in the KQ-AgNPs formation process[39]. The alkaline medium further facilitates the deportation of hydroxyl moieties to form highly reactive and nucleophilic phenoxide ions which reduce Ag^{+}[39]. Existing studies supports that usually catechol-containing molecules reduce metal ions to form NPs while simultaneously forming robust interfaces with metal surfaces[43]. These molecules coordinate strongly through adjacent hydroxyl groups and undergo oxidation to quinones, enabling covalent cross-linking via Michael addition and Schiff base reactions[50]. This redox coupling between metal ion reduction and catechol oxidation results in a stable polymeric shell around the NPs preventing them from aggregation. As reported by Gan et al. in the formation of Ag-lignin NPs, the mechanism involves the oxidation of catechol groups to o-quinones, which reduce Ag ions and stabilize the NPs through hydrogen bonding[50]. Inspired by these findings which are resembles to the phenol-metal-catechol redox chemistry observed in marine mussels and plant hydrogels, we hypothesize that similar interactions underlie the formation and exceptional stability of KQ-AgNPs. This dual action of reduction and stabilization provides a robust, green method for synthesizing highly stable AgNPs.

Antibacterial activity

Different parts of the papaya plant extracts have been widely reported for their antibacterial activity, primarily attributed to the rich phytochemical profile[23,24,33]. Numerous studies have documented the bactericidal properties of papaya-derived metabolites, highlighting their potential for biomedical applications. According to Dwivedi et al., statistical analysis revealed a significant difference in the flavonoid content across various extracts of papaya flowers[26]. These findings suggest that papaya flowers are abundant in flavonoid and phenolic compounds, which are the key contributors to their medicinal properties. Building on this knowledge, our study aimed to explore the synergistic action of KQE and AgNPs against four different bacterial isolates (Detailed procedure provided in Supplementary Information). In this study, we tested a comparative evaluation of antibacterial activity of KQE, KQ-AgNPs and AgNPs-Chem against four bacterial models: Fig. 5a–e represents the inhibition activity against various microorganisms: *S. aureus*, *B. subtilis*, *P. aeruginosa*, and *E. coli*. Figure 5e provides a comparative analysis of the inhibition activity of the samples against these tested microorganisms. The corresponding zone of inhibition diameters are recorded in Table 1.

The antibacterial activity of the samples at 16 µg/mL revealed that KQ-AgNPs demonstrated superior performance against all tested bacterial strains compared to KQE and Streptomycin. Notably, AgNPs-Chem

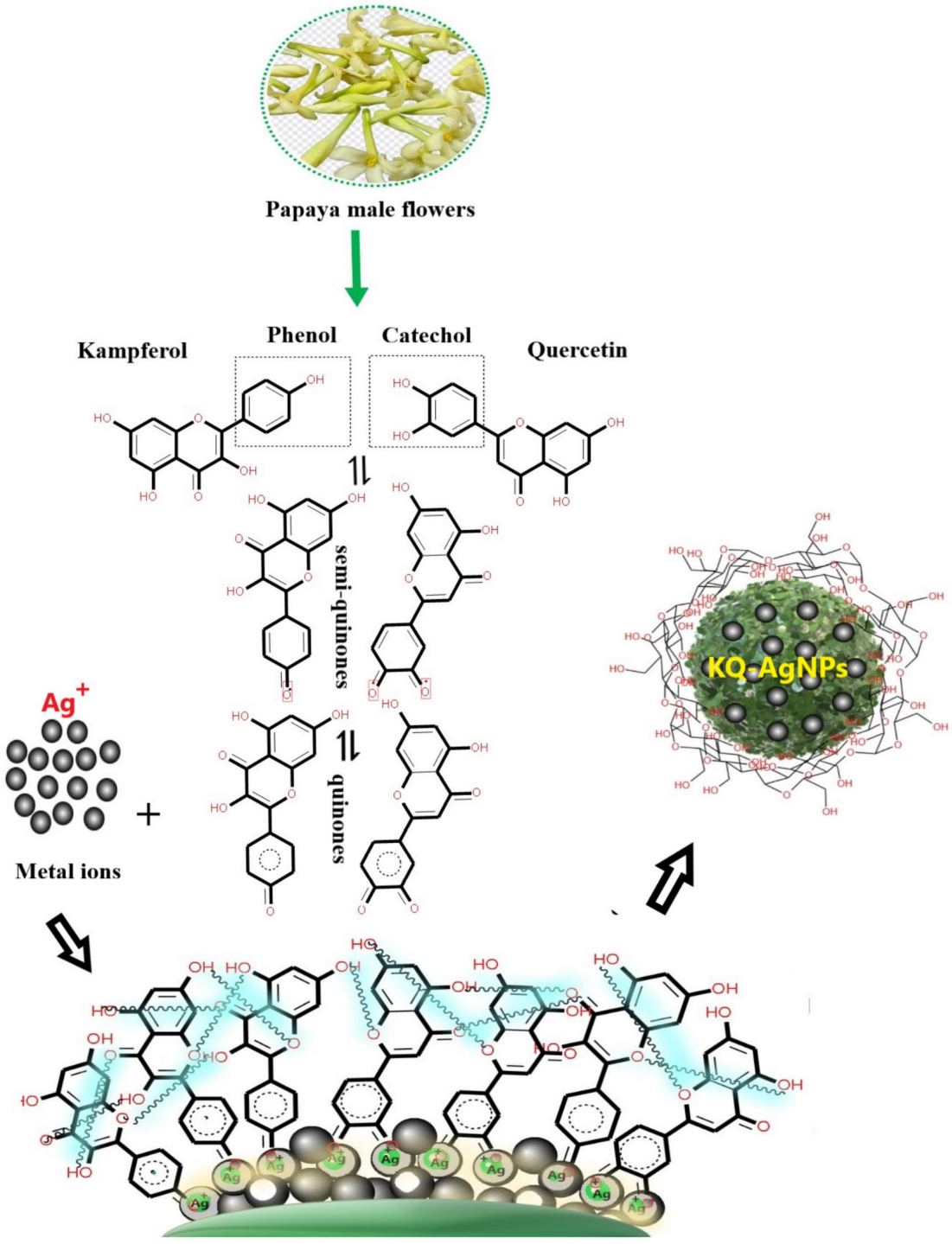

Fig. 4. Schematic representation of plausible mechanism of formation of KQ-AgNPs mediated by kaempferol and quercetin enriched KQE.

showed significant activity against *S. aureus* (9.84 mm), surpassing KQ-AgNPs (9.26 mm), although the latter exhibited comparable efficacy. KQ-AgNPs showed the highest zones of inhibition against *E. coli* (12.45 mm) and *P. aeruginosa* (11.76 mm), indicating enhanced efficacy, especially against gram-negative bacteria. This superior action can be attributed to the unique cell wall chemistry of gram-negative bacteria, which facilitates interactions between the NPs and the bacterial membrane, leading to increased disruption[17,26,34]. AgNPs synthesized using *Gmelina arborea* also shown similar kind of enhanced antibacterial activity against gram-negative bacteria, whereas in the case of *Smilax Chenensis* and *Moringa oleifera* the NPs were more resistant towards gram-positive strains[51–53].While KQE alone exhibited limited antibacterial activity, its combination with AgNPs suggesting a synergistic effect of its bioactive compounds with silver in KQ-AgNPs. Our findings align with previous

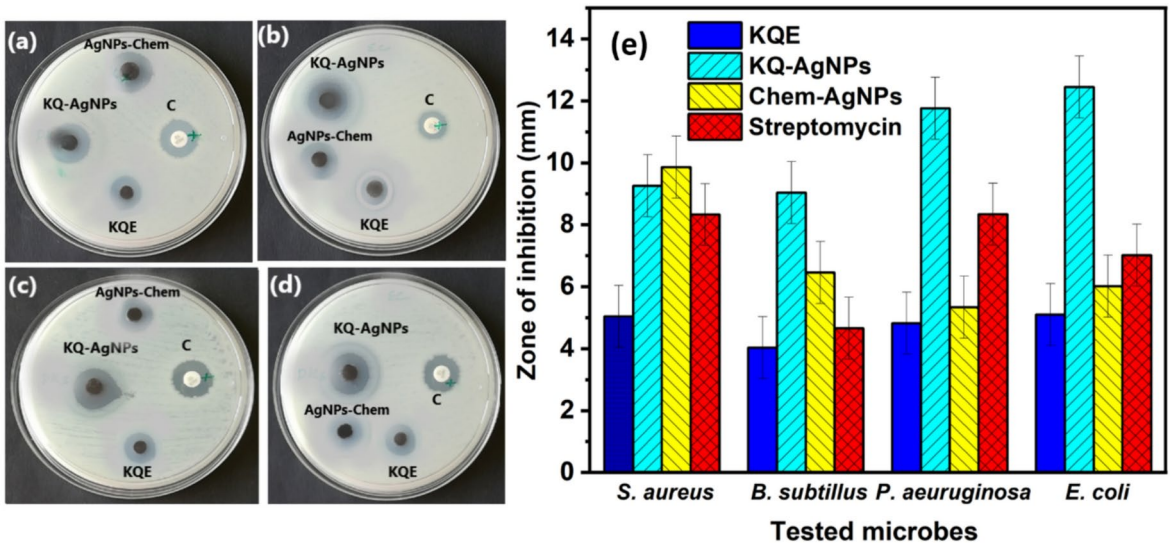

Fig. 5. The diameter of zone of inhibition show by of 16 µg/mL of KQE, KQ-AgNPs, AgNPs-Chem and streptomycine on bacterial samples (**a**) *S. aureus*, (**b**) *B. Subtillus*, (**c**) *P. aeuruginosa* and (**d**) *E. coli* and corresponding (**e**) comparative graphical representation.

Tested organisms	Diameter of zone of inhibition (mm) measured for (16 µg/mL)			Streptomycin (16 µg/mL) (mm)
	KQE	KQ-AgNPs	AgNPs-Chem	
S. aureus	5.04 ± 1.0	9.26 ± 1.0	9.84 ± 1.0	8.33 ± 1.0
B. subtillus	4.03 ± 1.0	9.04 ± 1.0	6.46 ± 1.0	4.66 ± 1.0
P. aeuruginosa	4.82 ± 1.0	11.76 ± 1.0	5.34 ± 1.0	8.34 ± 1.0
E. coli	5.10 ± 1.0	12.45 ± 1.0	6.02 ± 1.0	7.02 ± 1.0

Table 1. Zone diameter obtained for 16 µg/mL KQE, KQE-AgNPs, AgNPs-Chem and Streptomycine.

antibacterial research on AgNPs derived from three distinct varieties of Tulsi plants, demonstrating greater efficacy compared to their crude extracts[54]. Compared to AgNPs-Chem, KQ-AgNPs consistently outperformed in most cases, highlighting the advantages of green synthesis. Streptomycin, used as a standard, showed moderate activity but was surpassed by KQ-AgNPs in all the cases, underscoring the potential of these NPs as effective antibacterial agents. Similar studies by Jahangir et al. reported the synthesis of AgNPs using six different substrates of papaya, including leaf, seed, callus, peel, fruit juice, and bark. Among these, AgNPs derived from callus extract exhibited the most potent antimicrobial activity, with an inhibition zone of up to 19 mm against *Xanthomonas campestris* and 14 mm against *Aspergillus niger*[33]. These findings align with our observations, suggesting that the bioactive compounds in extracts prepared from different part of papaya plant play a critical role in enhancing the antimicrobial potential of AgNPs[31].

Figure 6a, b presents the SEM images of *E. coli* cells before and after treatment with KQ-AgNPs. The images clearly demonstrate significant physical damage to the bacterial cells, including cell wall disruption, shrinkage, aggregation, and increased surface roughness. Compared to chemically synthesized AgNPs generally NPs synthesized from biogenic sources exhibit a greater surface area due to the phytochemical capping around their surface[26,34]. This enhanced surface area facilitates more effective interactions with bacterial cells, contributing to the increased antibacterial impact observed. These interactions are schematically illustrated in Fig. 6c, which shows the sequence of events following bacterial exposure to KQ-AgNPs with biogenic capping provided from KQE. The NPs induce cell wall disruption, oxidative stress, leakage of intracellular contents, damage to internal cellular components, and inhibition of biofilm formation, ultimately leading to bacterial cell death. This comprehensive mechanistic depiction underscores the superior antibacterial efficacy of KQ-AgNPs compared to their chemically synthesized NPs.

As our KQ-AgNPs exhibit superior in vitro antibacterial activity against both gram-negative and gram-positive bacteria, they hold great potential for incorporation into antibacterial coatings, medical formulations, or packaging materials. However, compliance with industry standards and safety regulations must be evaluated, along with comprehensive in vivo testing to ensure safety and efficacy for real-world applications.

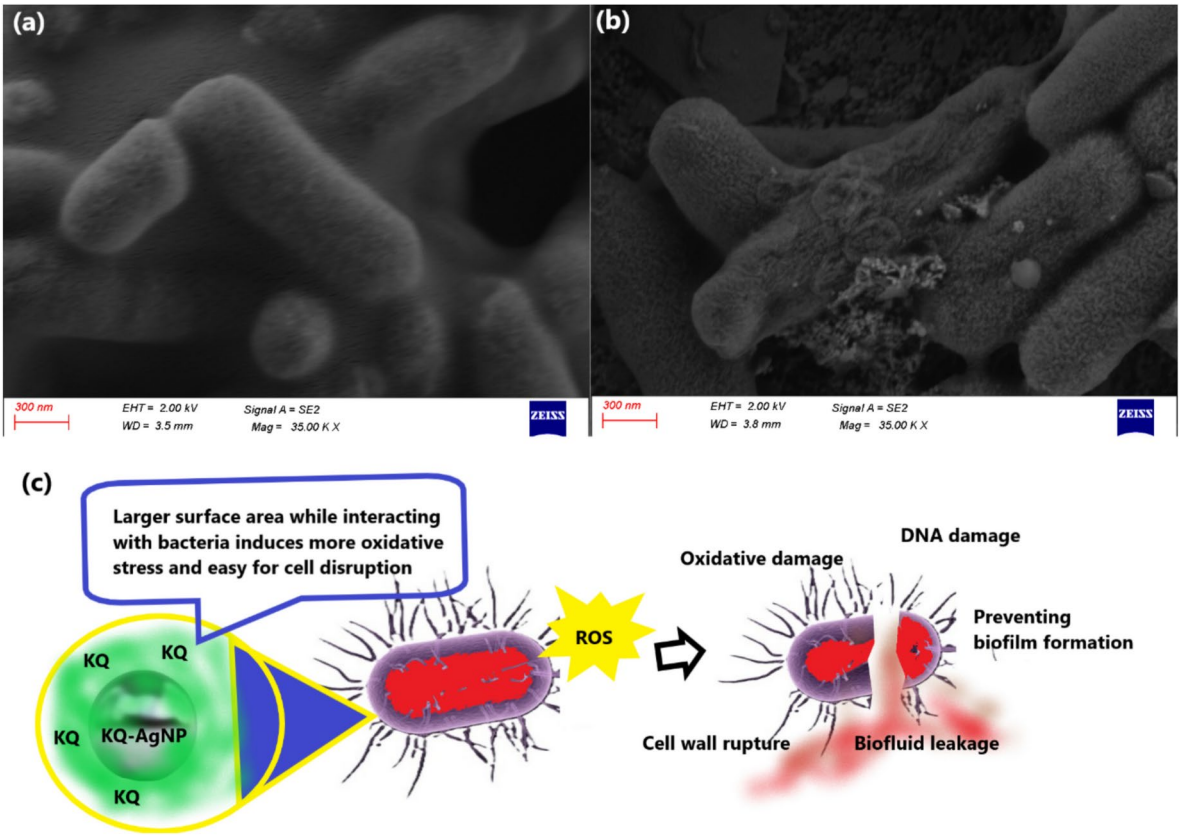

Fig. 6. SEM images of E. coli cells before (**a**) and after (**b**) treating with KQ-AgNPs. (**c**) Proposed antibacterial mechanism shown by KQ-AgNPs with biological capping of phytochemicals from KQE.

NPs	Papaya part used	Cancer cell type	Incubation time	IC_{50} value (µg/mL)	References
Se	Fruit	MCF-7	24 h	42.22 ± 3.21	55
		RAW 264.7		38.76 ± 2.68	
		Caco-2		42.85 ± 2.02	
MnCu co-doped NiO NPs)	Leaf	MDA-MB-231	24 h	23.97	56
AgNPs	Fruit peel	MCF-7	24 h	35.19 ± 3.58	35
		Hep-2	24 h	83.06 ± 4.47	
Di-methyl flubendazole mediate AgNPs	Leaf	HepG2	24 h	45.85	58
		MCF-7		51.37	
		A549		62.08	
AgNPs	Latex	MCF-7	48 h	19.88	59
AgNPs	Male flowers	MCF-7	24 h	21.25 ± 1.14	This work

Table 2. IC_{50} values of NPs reported in literature using papaya plant part as reducing/stabilizing agent.

Anticancer activity

Research shows that combining papaya plant extracts with metallic components significantly enhances their anticancer properties[44–60]. Metal-polyphenolic networks, including those formed with Ag, Au, Cu, Ni, Se, and other metals, have been synthesized using efficient, rapid, and eco-friendly methods[35,55,56,60]. These methods utilize extracts derived from various parts of the papaya tree, such as leaves, peels, bark, oil, fruit, and latex, all of which demonstrate promising anticancer activities.

Table 2 presents a comparative analysis of IC_{50} values reported in various studies for metallic NPs synthesized from different parts of the papaya plant. Inspired by these findings, this study investigates the anti-proliferative properties of KQ-AgNPs on MCF-7cells and compares them with AgNPs-Chem (Detailed procedure provided in Supplementary Information). The microscopic images Fig. 7a–e represent the inhibitory effect of KQ-AgNPs, while Fig. 7g–k depict the effects of AgNPs-Chem, showing progressive morphological changes in MCF-7 cells with increasing concentrations. Whereas, both Fig. 7f, l are control groups. The results clearly demonstrate that

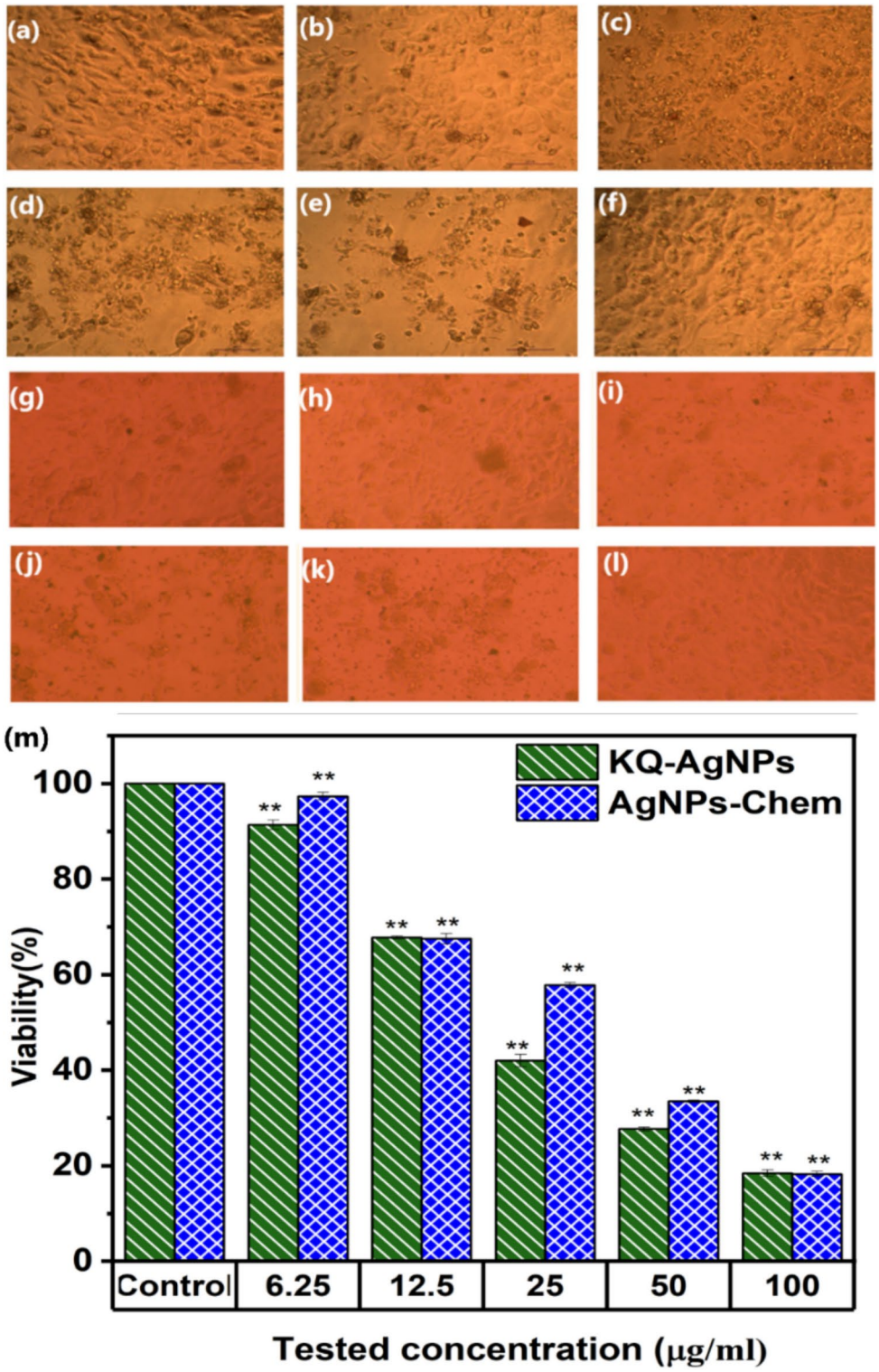

Fig. 7. Microscopic images representing the dose dependent inhibitory effect of KQ-AgNPs (**a**–**e**) and AgNPs-Chem (**g**–**k**) against MCF-7 cell lines with concentrations 6.25, 12.5, 25, 50 and 100 µg/mL respectively. (**f**, **l**) Control cells. (**m**) Viability (%) of KQ-AgNPs & AgNPs-Chem against MCF-7 for 24 h incubation period at concentrations 6.25, 12.5, 25, 50 and 100 µg/mL. ** refers to significant difference where $p < 0.01$.

the anticancer activity of both KQ-AgNPs and AgNPs-Chem are concentration-dependent. As shown in the microscopic images, the morphological changes in MCF-7 cells become progressively severe with increasing NP concentrations and highlighting cellular shrinkage, loss of adherence, and cell death at higher concentrations. This trend is further supported by the quantitative analysis in the bar graph Fig. 6m, which reveals a dose-

dependent reduction in cell viability. The IC_{50} value for KQ-AgNPs was calculated to be 21.25 ± 1.14 µg/mL, significantly lower than the IC_{50} value of 33.05 ± 3.13 µg/mL for AgNPs-Chem, indicating that KQ-AgNPs exhibit stronger cytotoxic effects against MCF-7 cells. Existing in-vivo experimental results by Nainggolan et al. and Sianipar et al. support the superior anticancer activity of papaya male flowers and align with our findings[28,57]. In alignment with our research, Qamar et al. demonstrated that AgNPs derived from *Ocimum basilicum L.* tea display enhanced anticancer efficacy against cervical immortalized (HeLa) cancer cells, yielding an IC_{50} value of 21.78 ± 0.68 µg/ml[61]. Another study looked into the exceptional anticancer activity of AgNPs made from *Vaccinium myrtillus* extract against human umbilical vein endothelial cells (HUVEC) and breast adenocarcinoma epithelial cells (MDA-MB-231)[62]. These studies provide evidence that AgNPs produced using more environmentally friendly methods have significant anticancer properties.

The lower IC_{50} value of KQ-AgNPs underscores their superior anticancer potency, further highlighting their potential for targeted anticancer therapy, where optimal dosing can achieve maximum therapeutic effects with minimal toxicity to healthy cells. In comparison, the study by Devanesan et al. on dimethyl flubendazole-extracted papaya leaf-derived AgNPs reported an IC_{50} value of 51.37 µg/mL against MCF-7 cells[58]. This is notably higher than the IC_{50} values observed in our work, suggesting that KQ-AgNPs are more effective at inducing cell death at lower concentrations. Papaya latex-reduced AgNPs on MCF-7 cells have also demonstrated comparable toxicity but required a longer incubation period, indicating a time-dependent effect[59]. While several studies have highlighted the strong anticancer activity of papaya-mediated AgNPs, a notable limitation is that effective concentrations against cancer cells often exhibit toxicity towards normal cells. In contrast, the IC_{50} value of our KQ-AgNPs against the HEK-293 cell line is 169.96 ± 2.3 µg/mL (Biocompatibility test results are provided in Figure S2 & S3 of SI), underscoring their selective nature and favorable safety profile. This selective toxicity towards cancer cells while sparing normal cells is consistent with the findings of Vundela et al. and Elderdery et al., who synthesized NPs using papaya fruit extracts[55,56].

The selective cytotoxicity of KQ-AgNPs can be attributed to a combination of factors. The inherent flavonoid enrich surface modification making them more biocompatible nature towards normal cells and toxic towards cancer cells by exhibiting antioxidant actions. On the other hand the negative surface charge of KQ-AgNPs, which influences cellular internalization and subcellular localization differently in normal and cancer cells. According to Asati et al., Cerium (Ce) NPs with a negative surface charge exhibit preferential internalization in cancer cells compared to normal cells[63]. This can be due to the altered membrane potential and increased expression of certain anionic transporter proteins in cancer cells, facilitating enhanced uptake of negatively charged NPs. In cancer cells, our KQ-AgNPs may be localized into the lysosomes leading to significant cytotoxicity. Whereas in the case of normal cells they may be accumulated in extracellular space or localizing in the cytoplasm without entering lysosomes thus resulting in lower cytotoxicity. This differential internalization and localization profile can be the reason for observed selective anticancer activity of KQ-AgNPs, making them highly potent against cancer cells while being biocompatible with normal cells. Our results indicate that KQ-AgNPs exhibit enhanced anticancer activity, suggesting their potential for targeted therapy. The lower IC_{50} value against cancer cells, coupled with a higher value against normal cells, reflects effective treatment with reduced toxicity.

The findings support the increasing recognition of biosynthesized KQ-AgNPs for their eco-friendly synthesis and bioactive properties, which contribute to their enhanced therapeutic efficacy in cancer treatment[64–66]. However, for large-scale production and biomedical applications, factors such as raw material accessibility, NPs stability, regulatory adherence, and economical manufacturing processes must be considered. Future initiatives will focus on process optimization, industry partnerships, and surface modifications (e.g., PEGylation) to enhance the biocompatibility, circulation time, and therapeutic efficacy of KQ-AgNPs, promoting their commercialization and clinical translation.

Conclusions

This study successfully demonstrates the green synthesis of highly stable KQ-AgNPs using a flavonol-enriched extract from male papaya flowers, an underutilized agricultural waste. The spherical KQ-AgNPs, with an average size of 12.3 ± 30 nm, exhibited remarkable stability for over three months without significant aggregation. The nanoparticles showed superior antibacterial activity, particularly against gram-positive bacteria, outperforming both the control and chemically synthesized AgNPs (AgNPs-Chem). Furthermore, KQ-AgNPs exhibited a significantly lower IC_{50} value (21.25 ± 1.14 µg/mL) against breast carcinoma cells compared to AgNPs-Chem and existing reports, highlighting their enhanced anticancer efficacy. This sustainable approach, leveraging natural flavonoid-rich extracts, offers a cost-effective and environmentally friendly alternative to commercially available flavonoid-based chemically reduced nanoparticles. The findings underscore the potential of KQ-AgNPs in biomedical applications and encourage further in vivo exploration and scalable production.

Data availability

Data are available from the corresponding author on reasonable request.

Received: 23 January 2025; Accepted: 10 March 2025
Published online: 15 March 2025

References

1. Magdy, G., Aboelkassim, E., Elhaleem, S. M. A. & Belal, F. A comprehensive review on silver nanoparticles: Synthesis approaches, characterization techniques, and recent pharmaceutical, environmental, and antimicrobial applications. *Microchem. J.* **196**, 109615 (2023).
2. Pryshchepa, O., Pomastowski, P. & Buszewski, B. Silver nanoparticles: Synthesis, investigation techniques, and properties. *Adv. Coll. Interface. Sci.* **284**, 102246 (2020).

3. Li, W.-R. et al. A comparative analysis of antibacterial activity, dynamics, and effects of silver ions and silver nanoparticles against four bacterial strains. *Int. Biodeterior. Biodegrad.* **123**, 304–310 (2017).
4. Carbone, M., Donia, D. T., Sabbatella, G. & Antiochia, R. Silver nanoparticles in polymeric matrices for fresh food packaging. *J. King Saud Univ. Sci.* **28**, 273–279 (2016).
5. ES, H. H., Bhattacharya, S., Varma, M. K. R. & Chandra, G. K. *Carica papaya* male flower mediated environmentally benign synthesis of silver nanoparticles towards the sensing of tryptophan. *Mater. Today Proc.* https://doi.org/10.1016/j.matpr.2023.03.731 (2023).
6. Gong, X. et al. An overview of green synthesized silver nanoparticles towards bioactive antibacterial, antimicrobial and antifungal applications. *Adv. Colloid Interface Sci.* **323**, 103053 (2023).
7. Khatoon, U. T., Velidandi, A. & Rao, G. V. S. N. Sodium borohydride mediated synthesis of nano-sized silver particles: Their characterization, anti-microbial and cytotoxicity studies. *Mater. Chem. Phys.* **294**, 126997 (2022).
8. Nemčeková, K., Svitková, V., Sochr, J., Gemeiner, P. & Labuda, J. Gallic acid-coated silver nanoparticles as perspective drug nanocarriers: Bioanalytical study. *Anal. Bioanal. Chem.* **414**, 5493–5505 (2022).
9. Ijaz, I., Gilani, E., Nazir, A. & Bukhari, A. Detail review on chemical, physical and green synthesis, classification, characterizations and applications of nanoparticles. *Green Chem. Lett. Rev.* **13**, 223–245 (2020).
10. Deng, S.-P. et al. Facile synthesis of long-term stable silver nanoparticles by kaempferol and their enhanced antibacterial activity against *Escherichia coli* and *Staphylococcus aureus*. *J. Inorg. Organomet. Polym Mater.* **31**, 2766–2778 (2021).
11. Jan, R. et al. Bioactivity and therapeutic potential of kaempferol and quercetin: New insights for plant and human health. *Plants* **11**, 2623 (2022).
12. Almatroudi, A. et al. Effects and mechanisms of Kaempferol in the management of cancers through modulation of inflammation and signal transduction pathways. *Int. J. Mol. Sci.* **24**, 8630 (2023).
13. Kim, D. H. et al. MicroRNA targeting by quercetin in cancer treatment and chemoprotection. *Pharmacol. Res.* **147**, 104346 (2019).
14. Sundaram, M. K., Hussain, A., Haque, S., Raina, R. & Afroze, N. Quercetin modifies 5′CpG promoter methylation and reactivates various tumor suppressor genes by modulating epigenetic marks in human cervical cancer cells. *J. Cell. Biochem.* **120**, 18357–18369 (2019).
15. Maghsoodloo, S. et al. Green synthesis of multifunctional silver nanoparticles using quercetin and their therapeutic potential. *DOAJ (DOAJ: Directory of Open Access Journals)* https://doi.org/10.22034/nmrj.2020.02.008 (2020).
16. Alrumaihi, F. et al. Pharmacological potential of kaempferol, a flavonoid in the management of pathogenesis via modulation of inflammation and other biological activities. *Molecules* **29**, 2007 (2024).
17. Anuar, A. H. H., Ghafar, S. A. A., Hanafiah, R. M., Lim, V. & Pazli, N. F. A. M. Critical evaluation of green synthesized silver nanoparticles-Kaempferol for antibacterial activity against methicillin-resistant *Staphylococcus aureus*. *Int. J. Nanomed.* **19**, 1339–1350 (2024).
18. Hwang, H. et al. Chronic ethanol exposure induces mitochondrial dysfunction and alters gene expression and metabolism in human cardiac spheroids. *Alcohol Clin. Exp. Res.* **47**, 643–658 (2023).
19. Bharathi, D. et al. Green synthesis of chitosan/silver nanocomposite using kaempferol for triple negative breast cancer therapy and antibacterial activity. *Environ. Res.* **238**, 117109 (2023).
20. Alyami, N. M., Alyami, H. M. & Almeer, R. Using green biosynthesized kaempferol-coated sliver nanoparticles to inhibit cancer cells growth: an in vitro study using hepatocellular carcinoma (HepG2). *Cancer Nanotechnol.* **13**, 26. https://doi.org/10.1186/s12645-022-00132-z (2022).
21. Asharani, P. V., Wu, Y. L., Gong, Z. & Valiyaveettil, S. Toxicity of silver nanoparticles in zebrafish models. *Nanotechnology* **19**, 255102 (2008).
22. Nguyen, T. et al. Chemical characterization and in vitro cytotoxicity on squamous cell carcinoma cells of *Carica papaya* leaf extracts. *Toxins* **8**, 7 (2015).
23. Miean, K. H. & Mohamed, S. Flavonoid (Myricetin, quercetin, kaempferol, luteolin, and apigenin) content of edible tropical plants. *J. Agricult. Food Chem.* **49**, 3106–3112 (2001).
24. Nugroho, A., Heryani, H., Choi, J. S. & Park, H.-J. Identification and quantification of flavonoids in *Carica papaya* leaf and peroxynitrite-scavenging activity. *Asian Pacific J. Trop. Biomed.* **7**, 208–213 (2016).
25. Sharma, S. et al. Forecasting the future of Papaya in India: predicting area and production through autoregressive integrated moving average. *Deleted J.* **66**, 183–191 (2023).
26. Dwivedi, M. K., Sonter, S., Mishra, S., Patel, D. K. & Singh, P. K. Antioxidant, antibacterial activity, and phytochemical characterization of *Carica papaya* flowers. *Beni-Suef Univ. J. Basic Appl. Sci.* **9**, 23. https://doi.org/10.1186/s43088-020-00048-w (2020).
27. Van, D. T. T., Cuong, D. H., Lien, G. T. K. & Yen, P. H. Phytochemical study of the ethyl acetate extract of male *Carica papaya* flowers from Quang Nam–Da Nang. *Vietnam J. Chem.* **58**, 145–150 (2020).
28. Nainggolan & Kasmirul. Cytotoxicity activity of male *Carica papaya* L. flowers on MCF-7 breast cancer cells. *J. Chem. Pharmaceut. Res.* **7**, 772–775.
29. Nga, V. T. et al. Ethanol extract of male *Carica papaya* flowers demonstrated non-toxic against MCF-7, HEP-G2, HELA, NCI-H460 cancer cell lines. *Vietnam J. Chem.* **58**, 86–91 (2020).
30. My, P. L. T. et al. Optimization of flavonoids extraction from vietnamese male papaya (*Carica papaya*, L.) flowers by ultrasound-asissted method and testing bioactivities of the extract. *ChemistrySelect* **5**, 13407–13416 (2020).
31 Lien, G. T. K. et al. A new phenolic constituent from *Carica papaya* flowers and its tyrosinase inhibitory activity. *Nat. Prod. Commun.* **14**, 1. https://doi.org/10.1177/1934578x19850987 (2019).
32. Purwaningsih & Indrayudha, P. A Systematic Review: Ethnomedicinal uses and pharmacological Activity of male papaya flower (*Carica papaya* L.). *Pharmacon J. Farmasi Indonesia* **21** (2024).
33. Jahangir, G. Z. et al. *Carica papaya* crude extracts are an efficient source of environmentally friendly biogenic synthesizers of silver nanoparticles. *Sustainability* **15**, 16633 (2023).
34. John, T., Parmar, K. A., Kotval, Sh. C. & Jadhav, J. Synthesis, characterization, antibacterial and anticancer properties of silver nanoparticles synthesized from *Carica papaya* peel extract. *Int. J. Nanosci. Nanotechnol.* **17**, 23–32 (2021).
35. Ohiduzzaman, M., Khan, M. N. I. & Khan, K. A. Green synthesis of *Carica papaya* mediated silver nanoparticles: Characterization, antibacterial activity, and bioelectricity generation for sustainable applications in nanotechnology. *J. Mol. Struct.* **1317**, 139141 (2024).
36. Srinivas, K., King, J. W., Howard, L. R. & Monrad, J. K. Solubility and solution thermodynamic properties of quercetin and quercetin dihydrate in subcritical water. *J. Food Eng.* **100**, 208–218 (2010).
37. Speisky, H., Arias-Santé, M. F. & Fuentes, J. Oxidation of quercetin and kaempferol markedly amplifies their antioxidant, cytoprotective, and Anti-Inflammatory properties. *Antioxidants* **12**, 155 (2023).
38. Sahu, A. K. & Mishra, A. K. Photophysical behavior of plant flavonols galangin, kaempferol, quercetin, and myricetin in homogeneous media and the DMPC model membrane: Unveiling the influence of the B-Ring hydroxylation of flavonols. *J. Phys. Chem. B* **126**, 2863–2875 (2022).
39. Chen, G., Ma, X., Meng, F. & Li, G. The electron transfer reactivity of kaempferol and its interaction with amino acid residues. *Bioelectrochemistry* **72**, 169–173 (2008).
40. Qi, W., Qi, W., Xiong, D. & Long, M. Quercetin: its antioxidant mechanism, antibacterial properties and potential application in prevention and control of toxipathy. *Molecules* **27**, 6545 (2022).

41. Yang, B., Arai, K. & Kusu, F. Electrochemical behaviors of quercetin and kaempferol in neutral buffer solution. *Anal. Sci.* **17**, 987–989 (2001).
42. Doak, J., Gupta, R. K., Manivannan, K., Ghosh, K. & Kahol, P. K. Effect of particle size distributions on absorbance spectra of gold nanoparticles. *Physica E Low-Dimens. Syst. Nanostruct.* **42**, 1605–1609 (2010).
43. Haridas, E. S. H., Bhattacharya, S., Varma, M. K. R. & Chandra, G. K. Bioinspired 5-caffeoylquinic acid capped silver nanoparticles using Coffee arabica leaf extract for high-sensitive cysteine detection. *Sci. Rep.* **13**, 8651. https://doi.org/10.1038/s41598-023-34944-9 (2023).
44. Ghasemi, S. et al. Process optimization for green synthesis of silver nanoparticles using Rubus discolor leaves extract and its biological activities against multi-drug resistant bacteria and cancer cells. *Sci. Rep.* **14**, 4130. https://doi.org/10.1038/s41598-024-54702-9 (2024).
45. Lem, O., Yoon, S., Bae, S. & Lee, W. The enhanced reduction of bromate by highly reactive and dispersive green nano-zerovalent iron (G-NZVI) synthesized with onion peel extract. *RSC Adv.* **11**, 5008–5018 (2021).
46 Baranović, G. & Šegota, S. Infrared spectroscopy of flavones and flavonols. Reexamination of the hydroxyl and carbonyl vibrations in relation to the interactions of flavonoids with membrane lipids. *Spectrochim. Acta Part A Mol. Biomol. Spectroscopy* **192**, 473–486 (2017).
47. Krysa, M., Szymańska-Chargot, M. & Zdunek, A. FT-IR and FT-Raman fingerprints of flavonoids—A review. *Food Chem.* **393**, 133430 (2022).
48 Simunkova, M. et al. Antioxidant vs. prooxidant properties of the flavonoid, kaempferol, in the presence of Cu(II) ions: A ROS-scavenging activity, fenton reaction and DNA damage study. *Int. J. Mol. Sci.* **22**, 1619 (2021).
49. Chand, K. et al. Green synthesis, characterization and photocatalytic application of silver nanoparticles synthesized by various plant extracts. *Arab. J. Chem.* **13**, 8248–8261 (2020).
50. Gan, D. et al. Plant-inspired adhesive and tough hydrogel based on Ag-Lignin nanoparticles-triggered dynamic redox catechol chemistry. *Nat. Commun.* **10**, 1487. https://doi.org/10.1038/s41467-019-09351-2 (2019).
51. Chandrasekharan, S., Chinnasamy, G. & Bhatnagar, S. Sustainable phyto-fabrication of silver nanoparticles using Gmelina arborea exhibit antimicrobial and biofilm inhibition activity. *Sci. Rep.* **12**, 156. https://doi.org/10.1038/s41598-021-04025-w (2022).
52. Gaddam, S. A. et al. Bioinspired multifunctional silver nanoparticles by Smilax Chenensis and their enhanced biomedical and catalytic applications. *Sci. Rep.* **14**, 29909. https://doi.org/10.1038/s41598-024-77071-9 (2024).
53. Shalaby, E. A., Shanab, S. M. M., El-Raheem, W. M. A. & Hanafy, E. A. Biological activities and antioxidant potential of different biosynthesized nanoparticles of Moringa oleifera. *Sci. Rep.* **12**, 18400. https://doi.org/10.1038/s41598-022-23164-2 (2022).
54. Alex, A. M. et al. Green synthesis of silver nanoparticle prepared with Ocimum species and assessment of anticancer potential. *Sci. Rep.* **14**, 11707. https://doi.org/10.1038/s41598-024-61946-y (2024).
55. Vundela, S. R. et al. Multi-biofunctional properties of phytofabricated selenium nanoparticles from *Carica papaya* fruit extract: antioxidant, antimicrobial, antimycotoxin, anticancer, and biocompatibility. *Front. Microbiol.* **12**, 769891. https://doi.org/10.3389/fmicb.2021.769891 (2022).
56. Alzahrani, B. et al. Manganese and copper-coated nickel oxide nanoparticles synthesized from *Carica papaya* leaf extract induce antimicrobial activity and breast cancer cell death by triggering mitochondrial caspases and p53. *Green Process. and Synthesis* **13**, 1–7. https://doi.org/10.1515/gps-2023-0087 (2024).
57 Sianipar, M. P., Suwarso, E. & Rosidah, R. Antioxidant And anticancer activities of hexane fraction from *Carica papaya* L. male flower. *Asian J. Pharmaceut. Clin. Res.* **11**, 81 (2018).
58. Devanesan, S., Jayamala, M., AlSalhi, M. S., Umamaheshwari, S. & Ranjitsingh, A. J. A. Antimicrobial and anticancer properties of *Carica papaya* leaves derived di-methyl flubendazole mediated silver nanoparticles. *J. Infect. Public Health* **14**, 577–587 (2021).
59. Chandrasekaran, R. et al. Formulation of *Carica papaya* latex-functionalized silver nanoparticles for its improved antibacterial and anticancer applications. *J. Mol. Liquids* **219**, 232–238 (2016).
60. Singh, S. P., Mishra, A., Shyanti, R. K., Singh, R. P. & Acharya, A. Silver nanoparticles synthesized using *Carica papaya* leaf extract (AgNPs-PLE) causes cell cycle arrest and apoptosis in human prostate (DU145) cancer cells. *Biol. Trace Element Res.* **199**, 1316–1331 (2020).
61 Qamar, S. U. R. et al. Silver nanoparticles from *Ocimum basilicum* L. tea: A green route with potent anticancer efficacy. *Colloids Interface Sci. Commun.* **59**, 100771 (2024).
62. Qamar, S. U. R. et al. Bioengineered silver nanoparticles suppress cancer and atherosclerosis by inducing oxidative stress. *BioNanoScience* **15**, 152. https://doi.org/10.1007/s12668-024-01782-6 (2024).
63. Asati, A., Santra, S., Kaittanis, C. & Perez, J. M. Surface-charge-dependent cell localization and cytotoxicity of cerium oxide nanoparticles. *ACS Nano* **4**, 5321–5331 (2010).
64. Anadozie, S. O., Adewale, O. B., Fadaka, A. O., Afolabi, O. B. & Roux, S. Synthesis of gold nanoparticles using extract of *Carica papaya* fruit: Evaluation of its antioxidant properties and effect on colorectal and breast cancer cells. *Biocatal. Agricult. Biotechnol.* **42**, 102348 (2022).
65. Nisa, F. Z., Astuti, M., Murdiati, A. & Haryana, S. M. Anti-proliferation and apoptosis induction of aqueous leaf extract of *Carica papaya* L. on human breast cancer cells MCF-7. *Pak. J. Biol. Sci.* **20**, 36–41 (2016).
66. Patel, S. et al. Anticancer activity of phytochemicals of the papaya plant Assessed: A Narrative review. *J. Cancer Prev.* **29**, 58–68 (2024).

Acknowledgements

The authors acknowledge the National Institute of Technology Calicut for providing comprehensive support for this study. E. S. H. H would like to sincerely thank Department of Science and Technology (DST), Govt. of India and SEM Centre, Department of Materials Science and Engineering, National Institute of Technology Calicut, for providing the facility purchased under the scheme 'Fund for Improvement of Science and Technology' (FIST—No. SR/FST/ET-I/2021/840) during the period of her project work.

Author contributions

Material preparation, data collection and analysis were performed by E. S. H. H. The first draft of the manuscript was written by E. S. H. H. M. K. R. V. revised the manuscript. G. K. C. supervised this work and revised the manuscript. All authors contributed to the article and agreed on the submitted version.

Declarations

Competing interests

The authors declare no competing interests.

Additional information

Supplementary Information The online version contains supplementary material available at https://doi.org/10.1038/s41598-025-93864-y.

Correspondence and requests for materials should be addressed to G.K.C.

Reprints and permissions information is available at www.nature.com/reprints.

Publisher's note Springer Nature remains neutral with regard to jurisdictional claims in published maps and institutional affiliations.